

Geometric analysis and formability of the cubic A_2BX_6 vacancy ordered double perovskite structure

Warda Rahim,^{a,b} Anjie Cheng,^a Chenyang Lyu,^a Tianyi Shi,^a Ziheng Wang,^a David O. Scanlon,^{a,b,c} Robert G. Palgrave^{a*}

a) Department of Chemistry, University College London, 20 Gordon Street, London, WC1H 0AJ

b) Thomas Young Centre, University College London, Gower Street, London WC1E 6BT, United Kingdom

c) Diamond Light Source Ltd., Diamond House, Harwell Science and Innovation Campus, Didcot, Oxfordshire OX11 0DE, United Kingdom

*corresponding author email: r.palgrave@ucl.ac.uk

Abstract

A geometric analysis of the cubic A_2BX_6 structure commonly formed by metal halides is presented. Using the 'hard sphere' approximation, where the ions are represented by spheres of a fixed radius, we derive four limiting models that each constrain the distances between constituent ions in different ways. We compare the lattice parameters predicted by these four models with experimental data from the Inorganic Crystal Structure Database (ICSD). For the fluorides, the maintenance of the AX bond length at the sum of the A and X radii gives the best approximation of the lattice parameter, leading to structures with widely separated BX_6 octahedra. For the heavier halides, a balance between forming an A site cavity of the correct size, and maintaining suitable anion-anion distances determines the lattice parameter. It is found that in many A_2BX_6 compounds of heavier halides, the neighbouring octahedra show very significant anion-anion overlap. We use these models to predict a compound with A site rattling and use DFT to confirm this prediction. Lastly, we use the geometric models to derive formability criteria for vacancy ordered double perovskites.

Introduction

Metal halide chemistry has undergone a renaissance in the past decade, led by the discovery and development of the halide perovskite solar cell absorbers. This class of materials, exemplified by $\text{CH}_3\text{NH}_3\text{PbI}_3$, possess some exceptional properties such as high optical absorption and efficient ambipolar charge transport and solution processability, which make them potentially transformative materials in the field of solar energy.¹⁻⁴ The intense interest in these perovskite metal halides has led to many related structures being revisited by researchers, both in search of similar functionality,⁵⁻⁸ and to further develop the understanding of fundamental features of the crystal chemistry of metal halide materials.⁹⁻¹¹ The *vacancy ordered double perovskite* structure, also known as the *defect perovskite* or K_2PtCl_6 structure, is a structure type formed by many compounds. Bearing a close similarity to the cubic perovskite structure, this cubic structure with general formula A_2BX_6 can be described as an ABX_3 perovskite with half of the B sites removed in an ordered fashion. A remarkable feature of this structure is its adoption by a very wide range of compositions, from fluorides to iodides, with no static tilting or reduction in symmetry as is seen very commonly in the ABX_3 perovskites. The vacancy ordered double perovskite structure is often described as consisting of isolated $[\text{BX}_6]^{2-}$ octahedra¹² with monovalent A site cations to balance charge, more in the fashion of a molecular crystal than an extended solid state structure. Despite this, some cubic A_2BX_6 compounds have been known for many years to be electronically conducting,¹³ and have recently been studied as solar cell absorbers themselves,^{8, 10, 14, 15} demonstrating good charge transport properties. This can be understood on the basis of electronic dimensionality, as opposed to structural dimensionality.¹⁶

Understanding the crystal chemistry of the ABX_3 perovskites has been the catalyst for the great number of applications and properties of that structure type.¹⁷ It may be that better understanding of the cubic A_2BX_6 likewise opens up new possibilities for building functional materials. Several authors have recently addressed fundamental crystal chemistry of this class of materials. For example, prediction of the lattice parameter of cubic A_2BX_6 structures from a given set of ions has been undertaken by several groups using a range of methodologies. Brik and Kityk used multiple linear regression to model the lattice parameter in terms of the ionic radii of each of the ions and the difference in electronegativity between the B and X ions.¹⁸ Sidey later simplified this approach, producing a linear model using only the ionic radii of each ion.¹⁹ Subsequently, Alade *et al.* used a support vector regression method to determine a model for the lattice parameter of cubic A_2BX_6 , which used as inputs the ionic radii and the electronegativities of all of the ions.²⁰ These approaches seek to find the best mathematical relationship between the lattice parameter and properties of the

constituent ions. They do not, however, take into account the geometric properties of the cubic A_2BX_6 structure itself, nor can they predict formability of the structure from a given set of ions.

The tolerance factor, t , for the ABX_3 perovskites is derived from a consideration of the geometry of the atoms in the ideal ABX_3 perovskite structure,¹⁷ given by:

$$t = \frac{r_A + r_X}{\sqrt{2}(r_B + r_X)}$$

The main structural difference between the ABX_3 perovskite and the cubic A_2BX_6 structure is that the latter has 50% of the B cations missing compared with the perovskite. The remaining B site cations form an ordered *fcc* arrangement, meaning that the BX_6 octahedra in the cubic A_2BX_6 structure are not connected by alternating B-X bonds; each anion is coordinated to only one B metal. For the cubic A_2BX_6 structure there is an additional degree of freedom compared with the perovskite, which can be expressed as the crystallographic x coordinate of the anion position. This represents the ability of the A_2BX_6 structure to vary to distance between BX_6 octahedra independently of their size. We have previously used an equation derived by Brown²¹ to understand the formation of Cs_2SnX_6 compounds ($X = \text{halide}$), and have shown that the tolerance factor is in fact a special case of Brown's equation.²² However, Brown's equation is in fact an approximation, since it assumes that in the coordination shell of the A site cation, the AX distance is always equal to the mean interanion distance, i.e. that the A site sits inside a perfect cuboctahedron of anions. This is not the case for most A_2BX_6 compounds.

Here we consider the geometry of the cubic A_2BX_6 structure in general, and highlight important differences compared with the ABX_3 perovskites. We define four limiting models, and by comparing the lattice parameters calculated with the experimental values from the Inorganic Crystal Structure Database (ICSD) we identify structural trends that occur across the range of compositions that form A_2BX_6 structures. We use these models to predict rattling in some cubic A_2BX_6 compounds, and use DFT calculations to test those predictions. We also propose a set of formability rules based on the geometric models we derive. Lastly we compare our approach with that of others, and discuss implications for materials design.

Methods

Structural data was obtained from the Inorganic Crystal Structure Database (ICSD). First principles calculations were carried out with the aim of understanding the rattling behaviour of selected materials. These were performed using pseudopotential plane-wave density functional theory²³ as implemented in the Vienna *Ab initio* Simulation Package (VASP).²⁴⁻²⁷ Interactions between core and valence electrons were described using the projector-augmented wave (PAW) method.²⁸ The PBEsol functional,²⁹ a variation of the Perdew-Burke-

Ernzerhof (PBE) generalised-gradient approximation (GGA) functional revised for solids,³⁰ was used for geometry optimisations and lattice dynamics calculations. Full details of computational methodology can be found in the Supporting Information.

Results

The first aim is to find an equation for the lattice parameter of cubic A_2BX_6 compounds in terms of the ionic radii, which is based on the geometry of the structure rather than a mathematical regression analysis. We also aim to produce a method to assess the formability of a cubic A_2BX_6 structure from a given set of A B and X ions. We will consider four limiting cases, and assess how each corresponds to the observed experimental lattice parameters of cubic A_2BX_6 compounds. In each case the distances between two pairs of ions is fixed at the sum of their ionic radii. We consider four relevant interatomic distances: AX, BX, XX and XX'. The latter two refer to the shortest distance between X anions coordinated to the same B site metal, and the shortest distance between X ions coordinated to different B metals, respectively.

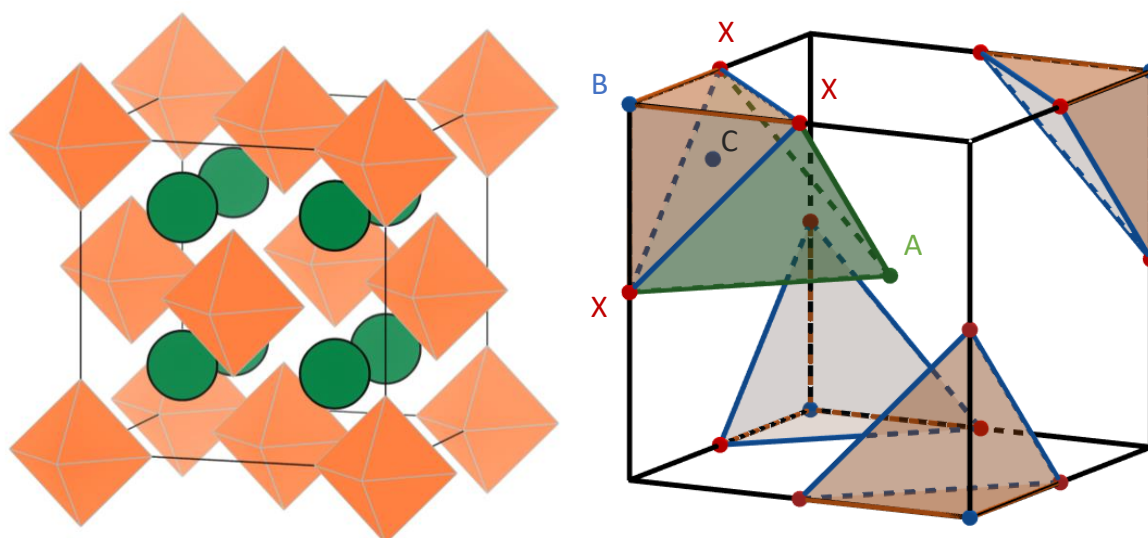


Figure 1. Left, unit cell of cubic A_2BX_6 structure showing A cations as green spheres and BX_6 octahedra. Right: One eighth of the cubic A_2BX_6 unit cell, showing the geometrical construction used to calculate the lattice parameter from the ion radii in Models 1 and 2, described in the text and Supplementary Information. Points A and B correspond to the centres of the A and B cation respectively. X corresponds to the three equivalent halide ions coordinated to both A and B. Point C is the centroid of the triangle XXX.

A useful way to think of this structure is as comprised of A and X ions that together form a cubic close packed arrangement. The B cations then sit in one quarter of the octahedral holes. If A and X are the same size, then their arrangement can, if we ignore the effect of the B site cation for now, be truly close packed, *i.e.* the distance AX being equal to XX, both being equal

to the sum of the ionic radii of A and X. In this case the X and A ions would just touch: each A ion being surrounded by a cuboctahedron of 12 X anions, and each X anion being surrounded by a cuboctahedron of 4 A cations and 8 X anions.

We now discuss four models, beginning with model 1. In this arrangement, the AX and BX bond lengths are set to be equal to the sum of the ionic radii, i.e. $r_X + r_A$ and $r_X + r_B$ respectively. The anions are either separated or overlapping as required to maintain the cation-anion bond lengths at the sum of the radii. We describe this model as the No Rattling (NR) model, as both the A and B cations fit exactly in their respective coordination shells. X anions are allowed to overlap with each other or be separated as required by maintenance of the AX and BX bond lengths at the sum of their radii. The lattice parameter can be calculated for model 1 as (derivation in the supporting information).

$$a = \frac{4}{\sqrt{3}} \left[\sqrt{(r_A + r_X)^2 - \frac{2}{3}(r_B + r_X)^2} + \frac{(r_B + r_X)}{\sqrt{3}} \right]$$

Model 2 is similar to model 1, except the BX distance is not fixed. Instead, the XX distance, that is, the distance between X anions coordinated to the same B site, is fixed at $2r_X$.

$$XX = 2r_X$$

This means the size of each $[BX_6]$ octahedron is determined only by the size of the anions, and the B site cation either rattles inside the cage if it is too small, or overlaps with the anions if too large. Utilising the other equations from model 1, the lattice parameter in model 2 is given by:

$$a = \frac{4}{\sqrt{3}} \left[\sqrt{(r_A + r_X)^2 - \frac{4}{3}r_X^2} + \sqrt{\frac{2}{3}}r_X \right]$$

It is notable that the lattice parameter calculated from model 2 is independent of r_B .

Model 3 fixes the BX bond length at $r_B + r_X$, meaning that the length XX is $\sqrt{2}(r_B + r_X)$ as in model 1. The XX' distance is fixed at $2r_X$, meaning that anions from neighbouring octahedra are just touching. The AX bond length unconstrained, potentially allowing the A site cation to rattle within its cage, or to overlap with the X anions in the coordination sphere.

The lattice parameter, which in model 3 is independent of r_A , can be derived from Figure S1 (Supplementary information) as:

$$a = 2(r_B + r_X) + 2\sqrt{2}r_X$$

Lastly, in model 4 both AX and BX are unconstrained by the ionic radii, meaning both cations can potentially rattle. Instead, XX and XX' are both set to the sum of the anionic radii. In this arrangement, the anions remain in their positions in the ideal close packed arrangement – all the anion nearest neighbour distances are the same and are equal to the sum of the anion radii; the anions just touch. If the A cation is smaller than the anion, it will rattle in its coordination cage. If the B site cation is smaller than the size of the octahedral hole, which is equal to $(\sqrt{2} - 1)r_X$, it too will rattle. If the A and B site cations are larger than these limits they will overlap with the anions. We will name this model the Anion Packing (AP) limit, and use this limit later to assess formability of cubic A_2BX_6 structures. In the AP limit, the equation for the lattice parameter is very simple and only dependent on r_X :

$$a = 4\sqrt{2}r_X$$

We now assess the accuracy of the lattice parameters predicted by the four models for the 110 unique cubic A_2BX_6 compounds in the ICSD. Firstly it should be noted that models 1 and 2, which both constrain the AX distance at $r_A + r_X$, produce very similar results for the compounds in Table 1, with an average difference between the predicted lattice parameter from models 1 and 2 for the same compound of 0.1%. Since the uncertainty of the ionic radii is likely larger than this value, we will not seek to differentiate between models 1 and 2, and will consider them together in comparison with models 3 and 4.

Model	Distances fixed at sum of ionic radii				Equation for lattice parameter
	AX	BX	XX	XX'	
1 'No Rattling' (NR)	Yes	Yes	No	No	$a = \frac{4}{\sqrt{3}} \left[\sqrt{(r_A + r_X)^2 - \frac{2}{3}(r_B + r_X)^2 + \frac{(r_B + r_X)}{\sqrt{3}}} \right]$
2	Yes	No	Yes	No	$a = \frac{4}{\sqrt{3}} \left[\sqrt{(r_A + r_X)^2 - \frac{4}{3}r_X^2 + \sqrt{\frac{2}{3}}r_X} \right]$
3	No	Yes	No	Yes	$a = 2(r_B + r_X) + 2\sqrt{2}r_X$
4 'Anion Packing' (AP)	No	No	Yes	Yes	$a = 4\sqrt{2}r_X$

Table 1. Equations for lattice parameters derived from the four models defined in the text.

The error for each compound is defined as $\frac{|a_{exp} - a_{calc}|}{a_{exp}}$, where a_{calc} is the calculated lattice parameter and a_{exp} is the experimental lattice parameter. Considering overall accuracy for the whole dataset, model 1 gives the best fit, with average error of 1.40% across all 110 compounds. This is larger than the error that can be achieved by a multiple linear regression model on a similar dataset (0.9%).¹⁹ However, there are significant variations across the dataset, and unlike the case of a purely mathematical regression model, we hope to show that comparing the various geometrical models with the experimental data gives insight into the structural diversity that exists within this set of compounds.

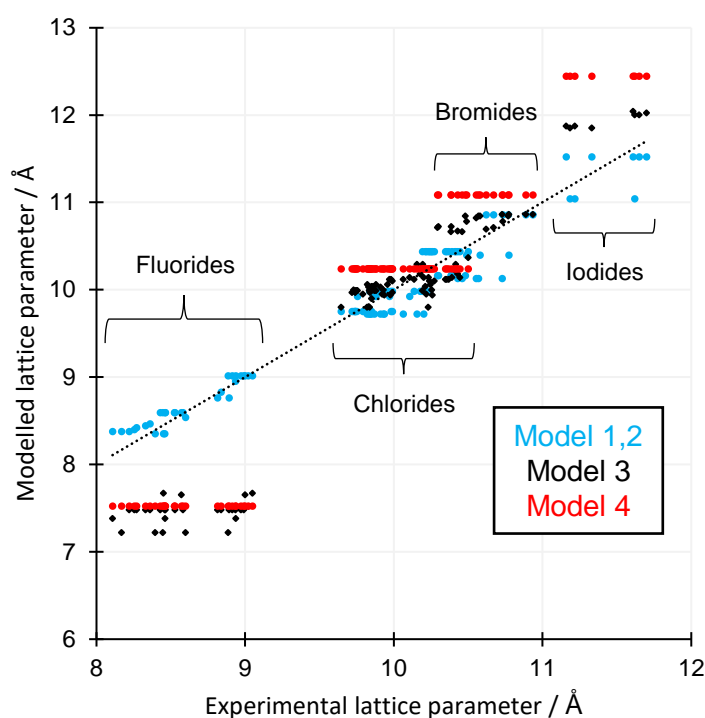


Figure 2. Experimental lattice parameters of the cubic A_2BX_6 compounds listed in the ICSD plotted against the prediction of the models described in the text. The dotted black line represents the experimental lattice parameters.

For the fluorides, the anion radius is significantly smaller than any of the A site cations that appear on the A site in Table S1. Thus if the AX distance is to be maintained at the sum of the ionic radii, then the anions on neighbouring octahedra must be well separated. This is in fact what is observed. Models 3 and 4 both assume the fluoride ions from different octahedra are separated by $2r_X$, *i.e.* the anions on neighbouring octahedra touch, and both models greatly underestimate the lattice parameter, by an average of 12.5% and 13.3% respectively. The large underestimate by models 3 and 4 of the lattice parameter show that the assumption of touching octahedra is incorrect, and in fact the separation between neighbouring octahedra is

much greater. Model 1 replicates the fluoride lattice parameters of the fluorides well, with average error of 1.05%. In this model, the A site fits exactly in the coordination sphere. Comparison with the models suggest that in all the A_2BF_6 compounds reported, the A site fits exactly within its coordination environment, which defines the lattice parameter, while the $[BF_6]$ octahedra are well separated.

Turning to the chlorides, a more complex picture emerges. In these compounds, $r_X = 1.81 \text{ \AA}$ and r_A can be slightly greater than this, in the case of $A = Cs^+$ ($r_A = 1.88 \text{ \AA}$) or smaller, for example in the case of Rb^+ , K^+ ($r_A = 1.72, 1.64 \text{ \AA}$ respectively). The lattice parameters of these, and the predictions from models 1-4 are shown in Figure 3. It is notable that in model 4, the Anion Packing model, the lattice parameter is independent of r_A and r_X , which means the predicted value of a is constant for all chloride compounds (indicated by the red line in Figure 3). Model 4 predicts $a = 4\sqrt{2}r_X = 10.239 \text{ \AA}$ for $r_X = 1.81 \text{ \AA}$. Chloride compounds with lattice parameters above this value must have some or all of the Cl anions separated, and conversely, those with lattice parameters below this value must have some or all of the Cl ions overlapping to some extent.

We will discuss compounds with the smaller cations, $A = Rb^+$, K^+ first. Because $r_A < r_X$, the largest lattice parameter that might be expected corresponds to model 4, with the largest ions, the chloride anions, touching and the smaller A and B sites allowed to rattle; all other models predict lower lattice parameters (for realistic values of r_B). Indeed, no experimental lattice parameter for the rubidium, potassium or ammonium chloride compounds listed in Table 1 exceeds that derived from model 4. It is found experimentally, however, that the lattice parameter in these compounds increases with increasing r_B , and this suggests that the B site cation does not rattle in these compounds, as otherwise its radius would have little or no impact on the lattice parameter. Indeed, model 3, which allows rattling A sites and non-rattling B sites, and has the anions of neighbouring octahedra touching, fits the data well for A_2BCl_6 with $A = Rb^+$ (figure 3, central panel). For these compounds, model 3 has smaller BX_6 octahedra than model 4, as model 3 allows anions within an octahedra to overlap in order to coordinate the small B site cation. For $A = K^+$, (Figure 3), model 3 reproduces the gradient of lattice parameter change with increasing r_B , but the actual experimental values of a are smaller than the model predicts. This may indicate that the anions of neighbouring octahedra in fact overlap, rather than just touch, or that some of the ionic radii concerned are incorrect, a point discussed below. We can conclude that of the models proposed, the best for A_2BCl_6 with $A = K^+$, Rb^+ is model 3 whereby the A site coordination environment is free to vary and BX bond length is fixed at the sum of the ionic radii. Note, that this latter condition means that chloride ions bound to the same B site metal overlap to some extent when $r_B < (\sqrt{2} - 1)r_X$, which is the case for

almost all chloride compounds in Table 1. For $A = K^+$, there also seems to be overlap between anions on neighbouring octahedra as well.

In contrast, the Cs_2BCl_6 compounds follow an altogether different pattern. Several compounds show lattice parameters very close to that predicted by model 4 ($a = 4\sqrt{2}r_X = 10.239 \text{ \AA}$ for $r_X = 1.81 \text{ \AA}$). For example, Cs_2WCl_6 ($a = 10.245 \text{ \AA}$),³¹ Cs_2GeCl_6 ($a = 10.21 \text{ \AA}$),³² Cs_2TiCl_6 ($a = 10.219 \text{ \AA}$)³³ all closely conform to model 4, despite their r_B values ranging from 0.53 - 0.66 \AA . In some Cs_2BCl_6 compounds, those with r_B greater than approximately 0.68 \AA , the lattice parameter exceeds that predicted by model 4, and in fact moves with increasing r_B toward the prediction of model 1 (Figure 3).

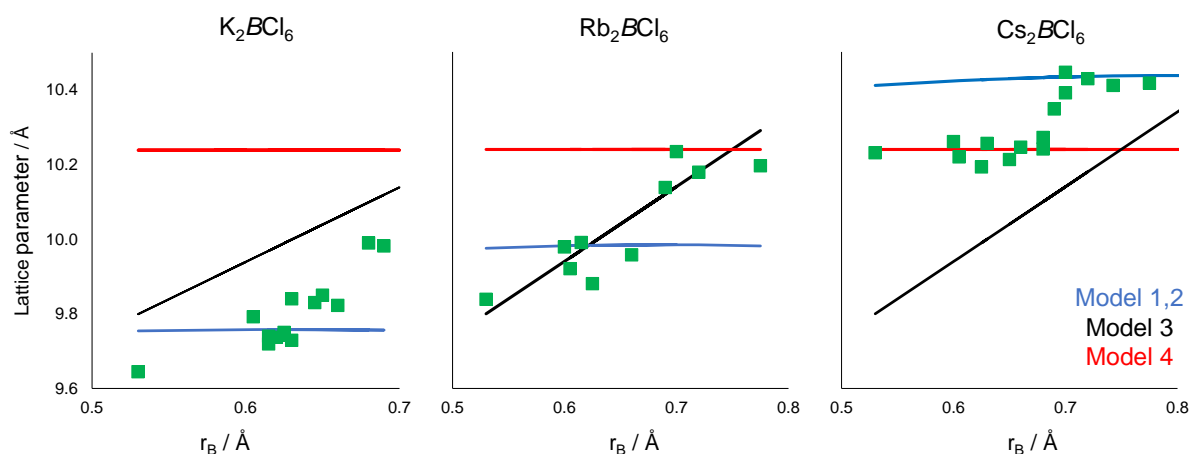


Figure 3. Experimental lattice parameter (green points) plotted against B site ionic radius (r_B) for cubic A_2BX_6 ($X = Cl$) and the A sites indicated, taken from the ICSD. Red lines indicate the prediction of model 4, the Anion Packing model, i.e. all the anions just touching. This model is independent of the A and B radii, hence gives the same prediction for all chloride compounds, and so these lines are horizontal. The black line indicates that prediction of model 3, in which anions within the same octahedron can overlap but those on different octahedra are separated by $2r_X$. The blue line shows the prediction from model 1, the No Rattling model, in which the AX and BX bond lengths are maintained at the sum of the relevant ionic radii.

There are fewer bromides in our dataset in Table S1, making general conclusions harder to draw. All of the A site ions we consider are smaller than bromide, and all of the B site cations are smaller than the size of the octahedral cavity formed by six bromide anions. Together this means that if the A-Br distance is set at the sum of the ionic radii (model 1), then the Br ions must overlap with each other. The corollary of course is that if the bromide anions are made to just touch (model 3 or 4), then the A site will rattle. The compounds of the smaller A site cations, ammonium and potassium, in fact fall between these two limits, with lattice

parameters almost midway between those predicted by models 1 and 3. This may indicate a situation with a degree of A site rattling, and some overlap of bromide anions on neighbouring octahedra. For compounds with Cs on the A site, the lattice parameters show dependence on r_B , and match closely with the predictions of model 3.

The iodides again have only a few examples in Table S1, which again makes general statements more difficult. For each compound listed, the anions are now much larger than either of the cations. These are likely to also be the most covalent compounds, due to the low electronegativity of iodide, and so we expect the Shannon ionic radii from the metal will be the most inaccurate. It is clear that the experimental lattice parameters are all very much smaller than predicted by model 4, the Anion Packing model, which would have all the iodide anions just touching ($a = 4\sqrt{2}r_X = 12.45 \text{ \AA}$ for $r_X = 2.20 \text{ \AA}$), and also model 3, which has the iodide anions on neighbouring octahedra just touching. Therefore, it seems certain that the anions are overlapping to a good degree in all the iodide compounds listed in Table 1, as may be expected for such soft and electropositive anion as iodide.

Model	Mean percentage error in predicted lattice parameter				
	Fluorides	Chlorides	Bromides	Iodides	Overall
1 and 2	1.05%	1.25%	2.18%	1.93%	1.40%
3	13.3%	1.57%	1.96%	4.45%	4.97%
4	12.5%	2.58%	4.82%	8.88%	6.03%

Table 2. Average accuracy of the lattice parameters of cubic A_2BX_6 derived from models 1-4. models 1 and 2 produce results that are very similar for all compounds considered, so are listed together.

Testing predictions of rattling ions

Rattling is an important property that can lead to low thermal conductivity or other phenomena, in perovskite oxides and halides and other structures.³⁴⁻³⁷ It arises when an ion is confined in a coordination environment larger than its radius. To assess the usefulness of these models in predicting real properties, not only lattice parameters, we consider which compounds are predicted to have rattling ions, according to the models presented here. Some series of compounds discussed above correspond well with the predictions of one or other of the models. The fluorides all generally align with model 1. The Rb_2BCl_6 compounds all match well with model 3, and the Cs_2BCl_6 compounds match with either model 1 or model 4. Since model 1 predicts no rattling, we move to models 3 and 4. Model 3 may have rattling A site cations, as the AX distance is not constrained. Model 4 may have either rattling A or B site cations, as neither metal halide distance is constrained. The Rb_2BCl_6 compounds all follow model 3 predictions of lattice parameter closely (Figure 3). Thus we can consider which of these

compounds is likely to have rattling A site. The AX distance predicted by model 3 for the Rb_2BCl_6 compounds can be compared with the sum of the ionic radii. If the predicted AX distance is larger than $r_A + r_X$, then we can predict the A site will rattle. Figure S2 shows the how the predicted AX values compare with $r_A + r_X$ for the Rb_2BCl_6 series. We choose two compounds for theoretical investigation: Rb_2GeCl_6 is predicted to have an AX distance of 3.45 Å, less than the sum of the radii which is 3.53 Å, suggesting the A site will not rattle, while Rb_2SnCl_6 has a predicted AX distance of 3.58 Å, which is greater than the sum of the radii. Thus we may expect Rb_2SnCl_6 to have a rattling A site. The phonon dispersion curves and the projected phonon density of states of the four compounds are shown in Figure 4. The vibrations of rattling atoms produce low-frequency optic modes in the phonon spectrum which undergo avoided crossing with the acoustic modes, modifying their dispersion and leading to low group velocities. This also results in increased phonon-phonon scattering and is responsible for low lattice thermal conductivity.³⁸⁻⁴⁰ The phonon dispersions in Figure 4 indicate this avoided crossing behaviour of the low-frequency optic modes with the acoustic modes. For both Rb_2GeCl_6 and Rb_2SnCl_6 , the low-frequency optic modes are dominated by Rb and Cl atom vibrations with very little mixing from Ge/Sn atom vibrations. At higher frequency it is predominantly Cl atom vibrations with small contributions from B-site cations (Ge/Sn). The average frequencies and average spring constants are listed in Table 3. The table also lists the ratio between minimum to maximum vibrational frequencies and spring constants. A small ratio of k_{\min} to k_{\max} connects with the idea of rattling, as it would indicate one of the atoms is much more weakly bonded compared to the rest and the decoupling of its motion from the other atoms would result in low-frequency optic phonon branches (Einstein modes).⁴¹ Weak chemical bonding is responsible for low phonon group velocities and therefore, low lattice thermal conductivity. In all cases, the A-site cations are acting as rattlers, and the lower spring constant for the Rb ion and smaller k_{\min}/k_{\max} in Rb_2SnCl_6 indicates that the Rb in this material rattles more compared to the A-site cations in Rb_2GeCl_6 and other compounds which will be discussed below. This agrees with the prediction of model 3, that Rb_2SnCl_6 has a larger A site cavity than Rb_2GeCl_6 . We also compare the calculated inter ionic distances with those predicted by model 3 for the two compounds, Table S3, and find good agreement: for example the AX distance matches within 0.029 Å for Rb_2GeCl_6 and 0.013 Å for Rb_2SnCl_6 .

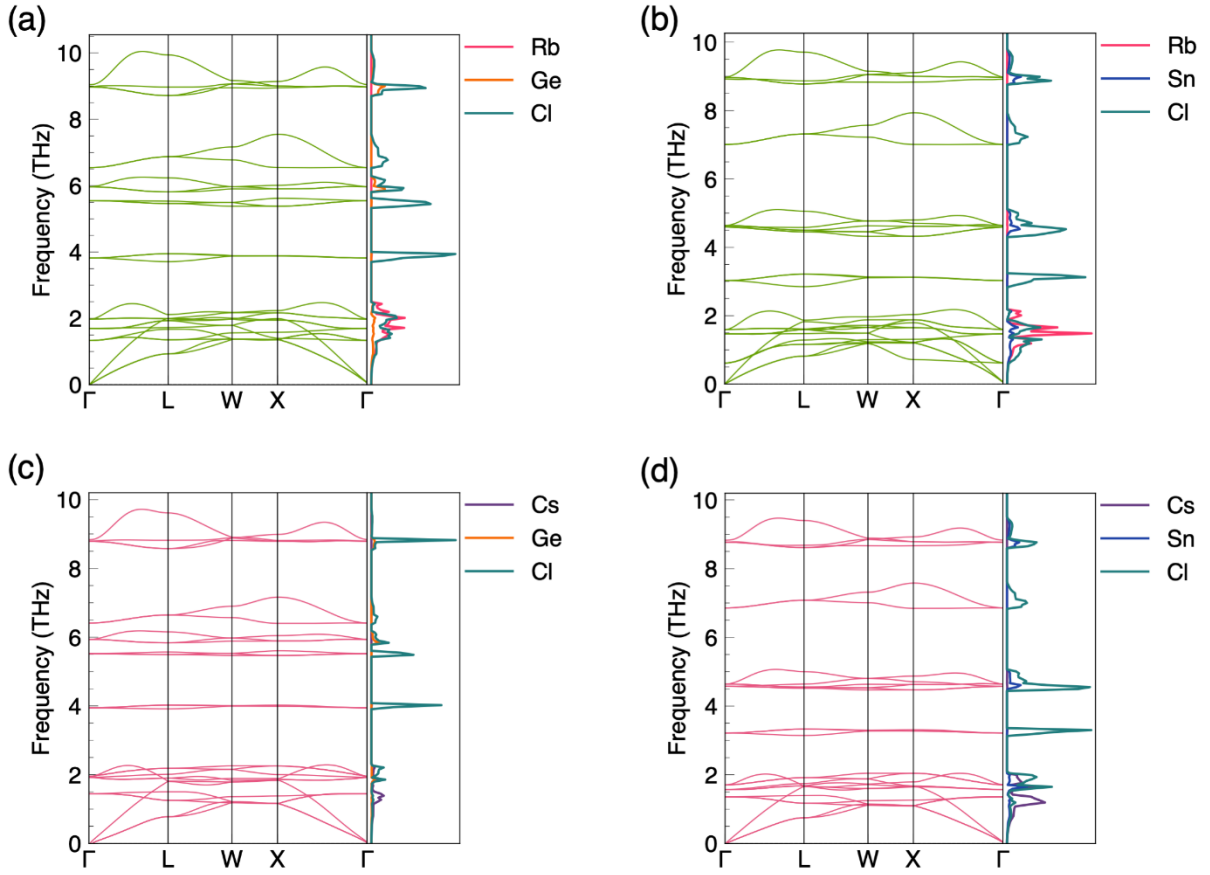


Figure 4. Figure 1: Phonon dispersions and projected density of states for (a) Rb_2GeCl_6 , (b) Rb_2SnCl_6 (c) Cs_2GeCl_6 and (d) Cs_2SnCl_6 .

We can carry out a similar analysis on the Cs_2BCl_6 compounds, which conform well to the lattice parameters of model 4, for smaller B site cations, and model 1 for larger ones. Model 4, the anion packing model, predicts a BX distance of $1.41r_X$, this is equal to 2.55 \AA . Thus any B site with a radius below $2.55 - 1.81 = 0.74 \text{ \AA}$ would be predicted by model 4 to be rattling. Cs_2GeCl_6 is such an example, with $r_B = 0.53 \text{ \AA}$. We calculate the vibrational modes of Cs_2GeCl_6 , and Cs_2SnCl_6 for comparison, which conforms most closely to the no rattling model (Figure 4). The projected density of states plots indicate that in case of Cs_2GeCl_6 and Cs_2SnCl_6 , the lowest frequency optic phonon branches are dominated by Cs atom vibrations, with the next highest having contributions from all 3 atoms, and in the higher frequency region it is predominantly Cl atom vibrations with very little contribution from Ge/Sn. Thus in contrast to the successful prediction of A site rattling from model 3, the prediction of B site rattling in Cs_2GeCl_6 is not born out by calculations. To see why this is, we can examine the inter ionic distances predicted by model 4 compared with those calculated by DFT (Table S3). While model 4 supposes that the anions are just touching ($XX = XX' = 3.62 \text{ \AA}$), in fact DFT reveals the anion sublattice is distorted, with $XX = 3.262 \text{ \AA}$ and $XX' = 3.728 \text{ \AA}$. The DFT calculated BX

distance corresponds closely with the sum of the radii, showing that the B site cation does not rattle within the octahedron, instead, the anions within one octahedron overlap to a large extent. Thus the agreement of the experimental lattice parameter of Cs_2GeCl_6 with the prediction of model 4 appears coincidental, and in fact the arrangement of ions is very close to that of model 1 (no rattling model), except that the AX distance is considerably shorter than the sum of the radii (3.613 Å vs 3.69 Å). This may be because of incorrect ionic radii, a theme discussed below, but also shows the disadvantage of using only lattice parameters to judge the models. A more robust approach would be to compare the experimental interionic distances with those predicted, but this is beyond the scope of this paper.

From the examples examined, we speculate that the Rb_2BCl_6 compounds may be a good series to explore for A site rattling. They seem to conform to model 3, and the larger B sites, with $r_B > 0.63$ Å, are all predicted to have an AX distance greater than the sum of the ionic radii. The known compounds this includes are Rb_2WCl_6 , Rb_2SnCl_6 , Rb_2TeCl_6 , Rb_2ZrCl_6 , Rb_2PbCl_6 .

Compound	ω_1	ω_2	ω_3	ω_{avg}	$\omega_{\text{min}}/\omega_{\text{max}}$	k_1	k_2	k_3	k_{avg}	$k_{\text{min}}/k_{\text{max}}$
Rb_2GeCl_6	1.77	5.95	4.94	4.37	0.30	4.44	42.70	14.34	20.50	0.10
Rb_2SnCl_6	1.50	4.58	4.38	3.72	0.33	3.21	41.35	11.28	18.61	0.08
Cs_2GeCl_6	1.48	5.92	5.50	4.84	0.25	4.80	42.24	17.83	21.62	0.11
Cs_2SnCl_6	1.37	4.47	4.44	3.73	0.31	4.17	39.42	11.59	18.39	0.11

Table 3. Average vibrational frequencies ω (THz), average spring constant k (N/m) for each atom, the ratio between minimum to maximum phonon frequency and spring constant in Rb_2GeCl_6 , Rb_2SnCl_6 , Cs_2GeCl_6 , and Cs_2SnCl_6 (Atom 1 corresponds to the A-site cation, atom 2 to the B-site cation, and atom 3 to the halide anion)

Formability of cubic A_2BX_6 structures

We turn now to the conditions for formability of cubic A_2BX_6 structures from a given set of A, B and X ions. As shown above, consideration of limiting models for the geometrical arrangement of the ions is a useful basis for understanding these structures, and so we follow this path in attempting to come up with criteria to predict formability of cubic A_2BX_6 structures. For ABX_3 perovskites, typically plots of tolerance factor vs the octahedral factor, μ , being the ratio $\frac{r_B}{r_X}$ have been successful^{42, 43} As we state above, the tolerance factor was devised to describe perovskites and the structural differences between cubic A_2BX_6 compounds and perovskites mean that caution must be used if applying the tolerance factor to non perovskite structures.

The criteria for formability we propose are linked to the limiting models described above. For each proposed A_2BX_6 composition, we calculate two geometric ratios. Firstly, using the ‘No Rattling’ (NR) model, model 1, which assumes that the AX bond length is set as $r_A + r_X$ and

the bond length BX is set at $r_B + r_X$, we calculate the distance between X anions of different octahedra, referred to as the XX'. We then express this distance as a proportion of the sum of the X ionic radii. Therefore on the horizontal axis we plot:

$$\frac{XX'}{2r_X}$$

A value above 1 for this ratio means that when the A and B ions fit exactly in their coordination sphere, the anions on neighbouring octahedra are not touching. When this ratio is below one, it means that for the A and B site cations fit exactly in their coordination sphere, the anions on neighbouring octahedra overlap. So on the horizontal axis we are asking the question – assuming the structure is optimised for the cation anion bond lengths, how separated are the anions from neighbouring octahedra, as a proportion of their radii?

As the second ratio we take the Anion Packing (AP) model (model 3) of a sublattice of anions that are just touching, meaning that all nearest neighbour anion-anion distances are equal to $2r_X$. Given this assumption, we can calculate how well the A site cation can fit into its coordination environment, expressed as the AX distance divided by the sum of the A and X radii:

$$\frac{AX}{r_A + r_X}$$

A value of above 1 for this ratio means the A site is rattling inside its cavity when the anion sublattice is just touching. A value below one means that the A site cation overlaps with the surrounding anions when the X sublattice is just touching. A value equal to one means that the A cation and X anions together form a close packed arrangement. Therefore on the vertical axis we are asking the question – assuming the structure is optimised for the anions to be in their close packed positions, how well does the A site cation fit into the resulting cavity?

Plotting the table of known cubic A_2BX_6 compounds on these two axes leads to the structure map shown in Figure 5. Known cubic compounds fall almost exclusively into two quadrants of this diagram. The top left quadrant represents compounds where the anions are larger than the A site, and satisfying the A cation coordination distance causes the anions to overlap. The further to the left a compound sits, the more the anions must overlap in order to maintain the AX bond length. In the bottom right quadrant, when the A site cation is fitted exactly into its coordination sphere, there is separation between the neighbouring octahedra. This separation increases on moving to the right. All the fluorides and also the Cs_2BCl_6 compounds fall into this quadrant. Representative compounds, and visualisations of the A site coordination environment, are shown in Figure 5. The bottom left quadrant, where both ratios are below 1,

would represent compounds where the A cation is too large for its cavity in the AP model and the X anions are overlapping in the NR model. This may seem paradoxical, but it is possible to have combinations of ions that end up in this quadrant if the B site cation is large, since the B site cation size affects the XX' distance in the NR model. The top right quadrant would conversely represent structures where the A site cation is too big to fit in the packed arrangement of anions, and the anions are too large to coordinate the A site without overlapping in the NR model. Again, this is possible where the B site is very small

Lines of constant octahedral factor (μ) are shown in Figure 5. All known cubic A_2BX_6 compounds fall between the lines for $\mu = 0.45$ and $\mu = 0.28$. As discussed above, when $\mu < (\sqrt{2} - 1) \approx 0.41$, then the B site cation is too small to fit inside the octahedron of anions around it, and either rattles in its cage or the surrounding anions must overlap. Interestingly, for the ABX_3 perovskites, with $X = O^{2-}, F^-, Cl^-, Br^-, I^-$ there is very close adherence to the criterion $\mu > \sqrt{2} - 1$ for formability of a perovskite. Li *et al.* found that of 186 halide ABX_3 compounds surveyed, only 3 with $\mu < \sqrt{2} - 1$ formed perovskites.⁴³ It was also found that 197 ABO_3 compounds, none with $\mu < \sqrt{2} - 1$ formed perovskites.⁴² Thus it is perhaps surprising that for the cubic A_2BX_6 , in fact the upper limit for μ is 0.45, and most compounds have μ values significantly below the limit of $\sqrt{2} - 1$. A demonstration of the difference in formability between cubic ABX_3 and A_2BX_6 compounds is that $CaSiO_3$ does not form a cubic perovskite, whereas Cs_2SiF_6 does form a cubic K_2PtCl_6 structure. In both these examples the cubic structure requires the Si^{4+} ion to sit within a regular octahedron of anions that are a similar size ($r_{F^-} = 1.33 \text{ \AA}$, $r_{oxide} = 1.40 \text{ \AA}$). The explanation for this difference in formability is probably that in the cubic A_2BX_6 structure, each anion coordinates to only one B site cation, *i.e.* is only part of one BX_6 octahedron. This allows the six anions of an octahedron to overlap with each other in order to coordinate a small B site cation without affecting the coordination of the neighbouring B site. In the ABX_3 perovskites, each anion forms bonds to two B site cations, so cannot move to coordinate a smaller B site without lengthening the bond to the other B site cation to which it coordinates. Thus it appears that the reason for adherence to the rule of $\mu > \sqrt{2} - 1$ for ABX_3 perovskites is not that the anions are forbidden from overlapping, but that they must each bond to two B site cations. The lifting of the latter requirement in the cubic A_2BX_6 compounds allows μ values considerably less than $\sqrt{2} - 1$.

It should also be considered why so few cubic A_2BX_6 structures, but so many cubic ABX_3 structures, are known with μ above $\sqrt{2} - 1$. The fact that $\mu = 0.46$ seems to be an upper limit for compounds that are described best by different geometric models may indicate that this limit is somehow fundamental to the cubic A_2BX_6 structure and not related to whichever model

best describes an particular compound. The answer to this is not apparent to us and may rest on other considerations than just the ion sizes.

We also find that a bounding line at $\frac{XX'}{2r_X} = 0.85$ contains all of the known compounds in the top left quadrant. No examples of cubic A_2BX_6 compounds are known with $\frac{XX'}{2r_X}$ value below 0.85, so this represents the limit of the anion overlap that is possible in this structure. Together with the lines for $\mu = 0.46$ and $\mu = 0.28$ we find this bounds all the known cubic A_2BX_6 structures.

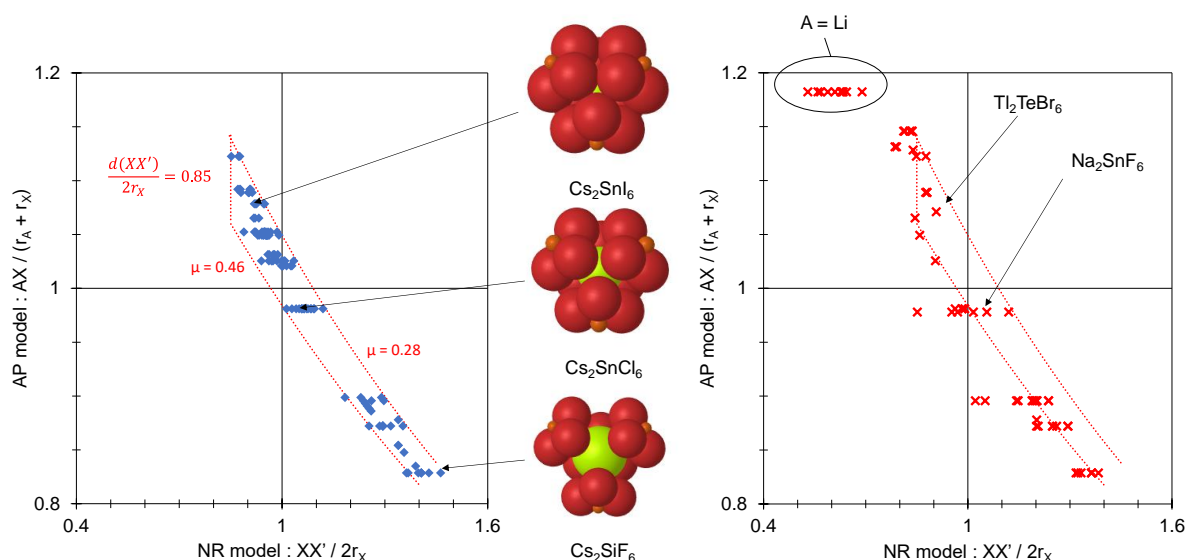


Figure 5. Structure map for cubic A_2BX_6 compounds. The horizontal axis plots the separation between anions on neighbouring octahedra when both A and B cations are perfectly coordinated (meaning that AX and BX bond lengths are set at the sum of the relevant ionic radii – this is the ‘No Rattling’ model). The vertical axis plots the separation between A and X ions when the anions are arranged in a close packed fashion (‘Anion Packing’ model). On the left hand plot, blue points represent known cubic compounds from ICSD (Table S1). Red lines represent the limits described in the text. Representations of the coordination around the A site viewed along a (111) direction for three compounds is shown, right (A site: green, B site: orange, X site: red) The right hand plot shows as red crosses the A_2BX_6 compounds from the ICSD that do not form a cubic structure (Table S2).

Also shown in the right hand panel of Figure 5 are points that correspond to all of the non-cubic compounds with A_2BX_6 composition in the ICSD; these are also listed in Table S2 in the supplementary information. Most of these points fall outside the marked area, but some do fall inside. For example, in the bottom right quadrant, some fluoride compounds have $\mu < 0.46$ yet are not cubic. Several Na_2BF_6 compounds are found within the marked region, yet none of these are cubic either. Only three heavier halide compounds are found within the marked area and yet are not cubic. These are K_2SnBr_6 , Tl_2TeBr_6 and Rb_2PdI_6 . Sidey *et al.* rationalise the

tetragonal distortion of Tl_2TeBr_6 in terms of the difficulty in packing the AX_3 sublattice, analogous to our models here.⁴⁴ It may be that the particular uncertainty in the Te ionic radius, discussed below, which might be corrected with further measurements, leads to this miscategorisation. Thus the prediction of formability gives few false positives for heavier halides, and more false positives for fluorides. It seems that fitting the fluorides into a scheme that also accounts for all the other halides is difficult. We have assessed numerous other structure mapping schemes, including taking into account electronegativity as Brik and Kityk have,¹⁸ yet we have found no better solution that is still based on geometry. Further discussion of some series of compounds and their relationship to these formability criteria is in the Supporting Information (Figure S3)

Discussion

As we have shown above, compounds that adopt the cubic A_2BX_6 structures show more structural diversity than might be expected for 'simple' cubic materials. All the fluorides adopt structures with well separated BX_6 octahedra, where the lattice parameter is determined by the maintenance of the AX bond length. For the fluorides, it is fair to describe the BX_6 octahedra as isolated molecular anions, given their large separation. In contrast, for the heavier halides, structures can be well described by anions from neighbouring octahedra just touching, leading the rattling A sites in some circumstances. All bromides and iodides considered here show smaller lattice parameters than the Anion Packing model predicts, showing that there must be considerable anion overlap in these materials. We conclude that, as has been previously asserted on electronic grounds,¹⁶ this means the description of these as having 'isolated octahedra' is less tenable than for the fluorides.

It has become popular to apply the Goldschmidt tolerance factor to structures related to the perovskites. For example, it has been applied to cubic A_2BX_6 structures by several authors in an effort to explain patterns of formability.^{45, 46} Of course, the tolerance factor was derived from geometric considerations of the perovskite structure, and whilst the cubic A_2BX_6 structure is similar, it has important differences, notably the possibility of the octahedra to change their separation independently of their size. In fact we have previously shown that in some compounds, the cubic A_2BX_6 structure does in fact distort in this way to preserve the AX distance at close to the sum of the radii, which clearly is impossible for the ABX_3 perovskite. We recently adapted the equation derived by Brown that describes the cavity size of the A site cation²¹ to show that the tolerance factor is in fact a special case of Brown's equation that can be generalised for A_2BX_6 structures.²² However, even our adaptation of Brown's radius ratio is an approximation, for it assumes that the AX bond length is always equal to the XX' distance, which is only true when the anion crystallographic coordinate $x = 0.25$ (i.e. when the A site

cation is coordinated by a perfect cuboctahedron). This assumption is approximately true for most compounds except the fluorides, where x typically deviates quite far from 0.25.

There are also two approaches to predicting lattice parameters or formability from ionic radii. The first is the geometric approach where relationships based on the ideal arrangement of atoms within the structure are derived. This is of course exemplified by the tolerance factor,^{47, 48} and it is the approach we have tried to take here. An alternative is to carry out mathematical regression to relate the lattice parameter or formability to the ionic radii of the ions. We have already mentioned examples of such methods for the A_2BX_6 structure,^{20, 49, 50} but another important example is the recent derivation of a 'new tolerance factor' for ABX_3 perovskites.⁵¹ This type of approach can be very accurate in calculating lattice parameters, or predicting formability, but comes with several drawbacks. Firstly, while some chemical principles can be inferred, nothing is learned directly from mathematical regression analysis about *why* the ionic radii influence the lattice parameter or formability in the way they do. A second serious problem that arises is to do with the set of ionic radii that are used. The Shannon radii have become ubiquitous for inorganic solid state chemistry, but a point sometimes overlooked is that the cation radii were derived from measurements of only oxides and fluorides.⁵² It is questionable how well they apply to metals bound to heavier, more electropositive, softer anions such as bromide and iodide, where assumptions of ions as hard spheres participating only in ionic bonding become tenuous to say the least. Shannon recognised this issue,⁵³ but it has still become common to use the unadjusted Shannon radii for all compounds, regardless of the chemical softness of the anion. We have previously calculated anion dependent ionic radii for a small selection of divalent metals relevant to ABX_3 perovskites using the same methodology as Shannon: calculating mean experimental bond lengths and fixing the anion radius to calculate the radius of the metal.⁵⁴ We found that some metals show large deviations from the Shannon radii when bound to heavy halides. For example Pb(II) has a much smaller radii when bound to iodide (1.03 Å) compared with when bound to oxide (1.19 Å), or put another way, the bond length of a Pb-I bond will be greatly overestimated if taken as the sum of the unadjusted Shannon radii. Input of such incorrect bond lengths, in the form of the unadjusted Shannon radii, into mathematical regression does not seem the best course. Another issue with mathematical regression analysis now emerges: equations derived from mathematical models trained with the unadjusted Shannon radii may appear to work well, but the value of any inference drawn from the form of the equations will be diminished, since the equations are the result of inaccurate inputs.

We attempted to replicate Shannon's method to derive anion adjusted radii values for the M^{4+} ions relevant to A_2BX_6 compounds. However, we encountered two problems, firstly, that not many examples of octahedrally coordinated M^{4+} chlorides, bromides and iodides are present

in the ICSD. Secondly, most of those which are present in the database are in fact cubic A_2BX_6 compounds. Furthermore, many older and some newer database entries are not characterised sufficiently (*i.e.* the anion crystallographic coordinate is not experimentally determined, and is typically set to 0.2500, and so the BX bond length cannot be determined), and even if they are, there is some uncertainty about whether the BX distance can always be taken as the sum of the ionic radii as we discuss above. Thus we have used the Shannon radii in this work, with only one exception (*infra*) but with the acknowledgement that future improvements in our knowledge of ionic radii of M^{4+} ions bound to heavy halides may change some of the conclusions here. The exception mentioned is with the radius of Te^{4+} , given by Shannon in an octahedral geometry as 0.97 Å. We find that this is clearly a large overestimate for halide compounds. In TeI_4 the Te-I mean bond length is 2.81 Å,⁵⁵ yielding a $r_{Te} = 0.61$ Å. In $TeCl_4$ the Te-Cl distance is 2.62 Å,⁵⁶ yielding $r_{Te} = 0.81$ Å. Without having enough accurately measured Te(IV) halide compounds in the ICSD, we are not able to calculate an exact value, but for this work have used $r_{Te(IV)} = 0.70$ Å for all compounds, but acknowledge this is a placeholder value until a more accurate radius can be measured. We anticipate that new, more accurate anion dependent radii for Te^{4+} and all the metals listed here will improve the understanding of A_2BX_6 and other halide structures. However, since we have used geometrical relationships rather than a mathematical regression, it should be possible to fit any newly derived radii into the models we introduce here.

Conclusion

We have derived geometrical models of the cubic A_2BX_6 , the vacancy ordered double perovskites. Whilst all the compounds considered here share the same space group, there is considerable diversity in their structures, which can be understood in terms for the four limiting models we introduce here. Whilst some compounds have isolated octahedra, in others, especially the bromides and iodides, there is significant overlap between anions. Geometric predictions of rattling A sites in Rb_2SnCl_6 was confirmed by DFT calculations. In terms of formability, it is interesting to note that the octahedral factor requirement for the cubic A_2BX_6 compounds is quite different from the ABX_3 perovskites. For ABX_3 perovskites it is a requirement to have an octahedral factor above 0.41, and this is often interpreted as avoid B site cation rattle or preventing anion overlap. However, it is very common for A_2BX_6 compounds to have an octahedral factor below 0.41, which challenges this explanation.

Acknowledgements

Via our membership of the UKs HEC Materials Chemistry Consortium, which is funded by EPSRC (EP/L000202, EP/R029431), this work used the ARCHER UK National Supercomputing Service (<http://www.archer.ac.uk>). We are also grateful to the UK Materials

and Molecular Modelling Hub for computational resources, which is partially funded by EPSRC (EP/P020194/1), and to UCL for access to the Kathleen (Kathleen@UCL) and Myriad (Myriad@UCL) supercomputers. WR is grateful to University College London for awarding the PhD scholarship.

Supporting information: Full computational methodology, tables of compounds in the datasets from the ICSD, full derivations of lattice parameters for model 1, further examples of formability criteria.

References

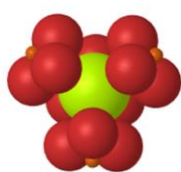
1. Sahli, F.; Werner, J.; Kamino, B. A.; Brauninger, M.; Monnard, R.; Paviet-Salomon, B.; Barraud, L.; Ding, L.; Leon, J. J. D.; Sacchetto, D.; Cattaneo, G.; Despeisse, M.; Boccard, M.; Nicolay, S.; Jeangros, Q.; Niesen, B.; Ballif, C., Fully textured monolithic perovskite/silicon tandem solar cells with 25.2% power conversion efficiency. *Nature Materials* **2018**, *17*, (9), 820-+.
2. Meggiolaro, D.; Motti, S. G.; Mosconi, E.; Barker, A. J.; Ball, J.; Perini, C. A. R.; Deschler, F.; Petrozza, A.; De Angelis, F., Iodine chemistry determines the defect tolerance of lead-halide perovskites. *Energy & Environmental Science* **2018**, *11*, (3), 702-713.
3. Li, Z.; Klein, T. R.; Kim, D. H.; Yang, M. J.; Berry, J. J.; van Hest, M.; Zhu, K., Scalable fabrication of perovskite solar cells. *Nature Reviews Materials* **2018**, *3*, (4).
4. Xing, G. C.; Mathews, N.; Sun, S. Y.; Lim, S. S.; Lam, Y. M.; Gratzel, M.; Mhaisalkar, S.; Sum, T. C., Long-Range Balanced Electron- and Hole-Transport Lengths in Organic-Inorganic CH₃NH₃PbI₃. *Science* **2013**, *342*, (6156), 344-347.
5. Lee, B.; Stoumpos, C. C.; Zhou, N. J.; Hao, F.; Malliakas, C.; Yeh, C. Y.; Marks, T. J.; Kanatzidis, M. G.; Chang, R. P. H., Air-Stable Molecular Semiconducting Iodosalts for Solar Cell Applications: Cs₂SnI₆ as a Hole Conductor. *Journal of the American Chemical Society* **2014**, *136*, (43), 15379-15385.
6. Saparov, B.; Sun, J. P.; Meng, W. W.; Xiao, Z. W.; Duan, H. S.; Gunawan, O.; Shin, D.; Hill, I. G.; Yan, Y. F.; Mitzi, D. B., Thin-Film Deposition and Characterization of a Sn-Deficient Perovskite Derivative Cs₂SnI₆. *Chemistry of Materials* **2016**, *28*, (7), 2315-2322.
7. Ganose, A. M.; Savory, C. N.; Scanlon, D. O., Beyond methylammonium lead iodide: prospects for the emergent field of ns(2) containing solar absorbers. *Chemical Communications* **2017**, *53*, (1), 20-44.
8. Lee, B.; Krenselewski, A.; Baik, S. I.; Seidman, D. N.; Chang, R. P. H., Solution processing of air-stable molecular semiconducting iodosalts, Cs₂SnI₆-xBr_x, for potential solar cell applications. *Sustainable Energy & Fuels* **2017**, *1*, (4), 710-724.
9. Xiao, Z. W.; Zhou, Y. Y.; Hosono, H.; Kamiya, T., Intrinsic defects in a photovoltaic perovskite variant Cs₂SnI₆. *Physical Chemistry Chemical Physics* **2015**, *17*, (29), 18900-18903.
10. Maughan, A. E.; Ganose, A. M.; Bordelon, M. M.; Miller, E. M.; Scanlon, D. O.; Neilson, J. R., Defect Tolerance to Intolerance in the Vacancy-Ordered Double Perovskite Semiconductors Cs₂SnI₆ and Cs₂TeI₆. *Journal of the American Chemical Society* **2016**, *138*, (27), 8453-8464.
11. Maughan, A. E.; Ganose, A. M.; Candia, A. M.; Granger, J. T.; Scanlon, D. O.; Neilson, J. R., Anharmonicity and Octahedral Tilting in Hybrid Vacancy-Ordered Double Perovskites. *Chemistry of Materials* **2018**, *30*, (2), 472-483.

12. Breternitz, J.; Schorr, S., What Defines a Perovskite? *Adv. Energy Mater.* **2018**, 8, (34), 1802366.
13. Suib, S.; Weller, P. F., SINGLE-CRYSTAL PREPARATION AND PROPERTIES OF CONDUCTING CS₂SN₆. *Abstracts of Papers of the American Chemical Society* **1975**, (169), 20-20.
14. Qiu, X. F.; Jiang, Y. A.; Zhang, H. L.; Qiu, Z. W.; Yuan, S.; Wang, P.; Cao, B. Q., Lead-free mesoscopic Cs₂Sn₆ perovskite solar cells using different nanostructured ZnO nanorods as electron transport layers. *Physica Status Solidi-Rapid Research Letters* **2016**, 10, (8), 587-591.
15. Kapil, G.; Ohta, T.; Koyanagi, T.; Vigneshwaran, M.; Zhang, Y. H.; Ogomi, Y.; Pandey, S. S.; Yoshino, K.; Shen, Q.; Toyoda, T.; Rahman, M. M.; Minemoto, T.; Murakami, T. N.; Segawa, H.; Hayase, S., Investigation of Interfacial Charge Transfer in Solution Processed Cs₂Sn₆ Thin Films. *Journal of Physical Chemistry C* **2017**, 121, (24), 13092-13100.
16. Maughan, A. E.; Ganose, A. M.; Scanlon, D. O.; Neilson, J. R., Perspectives and Design Principles of Vacancy-Ordered Double Perovskite Halide Semiconductors. *Chemistry of Materials* **2019**, 31, (4), 1184-1195.
17. Bhalla, A. S.; Guo, R. Y.; Roy, R., The perovskite structure - a review of its role in ceramic science and technology. *Mater. Res. Innov.* **2000**, 4, (1), 3-26.
18. Brik, M. G.; Kityk, I. V., Modeling of lattice constant and their relations with ionic radii and electronegativity of constituting ions of A(2)XY(6) cubic crystals (A=K, Cs, Rb, Tl; X=tetravalent cation, Y=F, Cl, Br, I). *Journal of Physics and Chemistry of Solids* **2011**, 72, (11), 1256-1260.
19. Sidey, V., A simplified empirical model for predicting the lattice parameters of the cubic/pseudocubic perovskites. *Journal of Solid State Chemistry* **2019**, 279.
20. Alade, I. O.; Olumegbon, I.; Bagudu, A., Lattice constant prediction of A(2)XY(6) cubic crystals (A = K, Cs, Rb, Tl; X = tetravalent cation; Y = F, Cl, Br, I) using computational intelligence approach. *Journal of Applied Physics* **2020**, 127, (1).
21. Brown, I. D., CRYSTAL STRUCTURE OF K₂TEBR₆. *Canadian Journal of Chemistry-Revue Canadienne De Chimie* **1964**, 42, (12), 2758-&.
22. Karim, M. M. S.; Ganose, A. M.; Pieters, L.; Leung, W. W. W.; Wade, J.; Zhang, L.; Scanlon, D. O.; Palgrave, R. G., Anion Distribution, Structural Distortion, and Symmetry-Driven Optical Band Gap Bowing in Mixed Halide Cs₂SnX₆ Vacancy Ordered Double Perovskites. *Chemistry of Materials* **2019**, 31, (22), 9430-9444.
23. Kohn, W.; Sham, L. J., Self-Consistent Equations Including Exchange and Correlation Effects. *Physical Review* **1965**, 140, (4A), A1133-A1138.
24. Kresse, G.; Hafner, J., Ab initio molecular dynamics for liquid metals. *Physical Review B* **1993**, 47, (1), 558-561.
25. Kresse, G.; Hafner, J., Ab initio molecular-dynamics simulation of the liquid-metal--amorphous-semiconductor transition in germanium. *Physical Review B* **1994**, 49, (20), 14251-14269.
26. Kresse, G.; Furthmüller, J., Efficient iterative schemes for ab initio total-energy calculations using a plane-wave basis set. *Physical Review B* **1996**, 54, (16), 11169-11186.
27. Kresse, G.; Furthmüller, J., Efficiency of ab-initio total energy calculations for metals and semiconductors using a plane-wave basis set. *Computational Materials Science* **1996**, 6, (1), 15-50.
28. Blöchl, P. E., Projector augmented-wave method. *Physical Review B* **1994**, 50, (24), 17953-17979.
29. Perdew, J.; Ruzsinszky, A.; Csonka, G.; Vydrov, O. A.; Scuseria, G.; Constantin, L.; Zhou, X.; Burke, K. In *Generalized gradient approximation for solids and their surfaces*, 2007; 2007.
30. Perdew, J. P.; Burke, K.; Ernzerhof, M., Generalized Gradient Approximation Made Simple. *Phys Rev Lett* **1996**, 77, (18), 3865-3868.
31. Wang, P.; Xu, W.; Zheng, Y.-Q., Crystal structure of dicaesium hexachlorotungstate(IV), Cs₂[WCl₆] %J Zeitschrift für Kristallographie - New Crystal Structures. **2003**, 218, (1), 25.
32. Laubengayer, A. W.; Billings, O. B.; Newkirk, A. E., Chlorogermanic acid and the chlorogermanates - Properties and crystal structure of cesium hexachlorogermanate. *Journal of the American Chemical Society* **1940**, 62, 546-548.

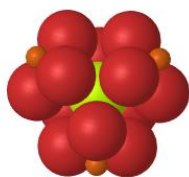
33. Engel, G., Die Kristallstrukturen einiger Hexachlorokomplexsalze %J Zeitschrift für Kristallographie - Crystalline Materials. **1935**, 90, (1), 341.
34. Lee, W.; Li, H. S.; Wong, A. B.; Zhang, D. D.; Lai, M. L.; Yu, Y.; Kong, Q.; Lin, E.; Urban, J. J.; Grossman, J. C.; Yang, P. D., Ultralow thermal conductivity in all-inorganic halide perovskites. *Proceedings of the National Academy of Sciences of the United States of America* **2017**, 114, (33), 8693-8697.
35. Kontos, A. G.; Kaltzoglou, A.; Arfanis, M. K.; McCall, K. M.; Stoumpos, C. C.; Wessels, B. W.; Falaras, P.; Kanatzidis, M. G., Dynamic Disorder, Band Gap Widening, and Persistent Near-IR Photoluminescence up to At Least 523 K in A₃SnI₃ Perovskites (A = Cs⁺, CH₃NH₃⁺ and NH₂-CH=NH₂⁺). *Journal of Physical Chemistry C* **2018**, 122, (46), 26353-26361.
36. Straus, D. B.; Guo, S.; Abeykoon, A. M. M.; Cava, R. J., Understanding the Instability of the Halide Perovskite CsPbI₃ through Temperature-Dependent Structural Analysis. *Advanced Materials* **2020**, 32, (32).
37. Xie, H. Y.; Hao, S. Q.; Bao, J. K.; Slade, T. J.; Snyder, G. J.; Wolverton, C.; Kanatzidis, M. G., All-Inorganic Halide Perovskites as Potential Thermoelectric Materials: Dynamic Cation off-Centering Induces Ultralow Thermal Conductivity. *Journal of the American Chemical Society* **2020**, 142, (20), 9553-9563.
38. Dong, J.; Sankey, O. F.; Ramachandran, G. K.; McMillan, P. F., Chemical trends of the rattling phonon modes in alloyed germanium clathrates. **2000**, 87, (11), 7726-7734.
39. Lin, H.; Tan, G.; Shen, J.-N.; Hao, S.; Wu, L.-M.; Calta, N.; Malliakas, C.; Wang, S.; Uher, C.; Wolverton, C.; Kanatzidis, M. G., Concerted Rattling in CsAg₅Te₃ Leading to Ultralow Thermal Conductivity and High Thermoelectric Performance. **2016**, 55, (38), 11431-11436.
40. Juneja, R.; Singh, A. K., Rattling-Induced Ultralow Thermal Conductivity Leading to Exceptional Thermoelectric Performance in AgIn₅S₈. *ACS Appl. Mater. Interfaces* **2019**, 11, (37), 33894-33900.
41. Feng, Z.; Fu, Y.; Zhang, Y.; Singh, D. J., Characterization of rattling in relation to thermal conductivity: Ordered half-Heusler semiconductors. *Physical Review B* **2020**, 101, (6), 064301.
42. Li, C.; Soh, K. C. K.; Wu, P., Formability of ABO₃ perovskites. *Journal of Alloys and Compounds* **2004**, 372, (1-2), 40-48.
43. Li, C.; Lu, X.; Ding, W.; Feng, L.; Gao, Y.; Guo, Z., Formability of ABX₃ (X = F, Cl, Br, I) halide perovskites. *Acta Crystallographica Section B-Structural Science Crystal Engineering and Materials* **2008**, 64, 702-707.
44. Sidey, V. I.; Zubaka, O. V.; Solomon, A. M.; Kun, S. V.; Peresh, E. Y., X-ray powder diffraction studies of Ti₂TeBr₆ and Ti₂TeI₆. *Journal of Alloys and Compounds* **2004**, 367, (1), 115-120.
45. Fedorovskiy, A. E.; Drigo, N. A.; Nazeeruddin, M. K., The Role of Goldschmidt's Tolerance Factor in the Formation of A₂BX₆ Double Halide Perovskites and its Optimal Range. *Small Methods* **0**, (0), 1900426.
46. Maughan, A. E.; Ganose, A. M.; Almaker, M. A.; Scanlon, D. O.; Neilson, J. R., Tolerance Factor and Cooperative Tilting Effects in Vacancy-Ordered Double Perovskite Halides. *Chemistry of Materials* **2018**, 30, (11), 3909-3919.
47. Filip, M. R.; Giustino, F., The geometric blueprint of perovskites. *Proceedings of the National Academy of Sciences* **2018**, 115, (21), 5397.
48. Goldschmidt, V. M., The laws of crystal chemistry. *Naturwissenschaften* **1926**, 14, 477-485.
49. Sidey, V., A simplified empirical model for predicting the lattice parameters for the cubic perovskite-related inorganic A₂BX₆ halides. *Journal of Physics and Chemistry of Solids* **2019**, 126, 310-313.
50. Cai, Y.; Xie, W.; Ding, H.; Chen, Y.; Thirumal, K.; Wong, L. H.; Mathews, N.; Mhaisalkar, S. G.; Sherburne, M.; Asta, M., Computational Study of Halide Perovskite-Derived A₂BX₆ Inorganic Compounds: Chemical Trends in Electronic Structure and Structural Stability. *Chemistry of Materials* **2017**, 29, (18), 7740-7749.

51. Bartel, C. J.; Sutton, C.; Goldsmith, B. R.; Ouyang, R. H.; Musgrave, C. B.; Ghiringhelli, L. M.; Scheffler, M., New tolerance factor to predict the stability of perovskite oxides and halides. *Science Advances* **2019**, *5*, (2).
52. Shannon, R. D., REVISED EFFECTIVE IONIC-RADII AND SYSTEMATIC STUDIES OF INTERATOMIC DISTANCES IN HALIDES AND CHALCOGENIDES. *Acta Crystallographica Section A* **1976**, *32*, (SEP1), 751-767.
53. Shannon, R. D.; Gumerman, P. S., EFFECT OF COVALENCE ON INTERATOMIC DISTANCES IN CU+, AG+, TI+ AND PB2+ HALIDES AND CHALCOGENIDES. *Journal of Inorganic & Nuclear Chemistry* **1976**, *38*, (4), 699-703.
54. Travis, W.; Glover, E. N. K.; Bronstein, H.; Scanlon, D. O.; Palgrave, R. G., On the application of the tolerance factor to inorganic and hybrid halide perovskites: a revised system. *Chemical Science* **2016**, *7*, (7), 4548-4556.
55. Krebs, B.; Paulat, V., Kristallstruktur des Tellurtetraiodids TeI₄. *Acta Crystallographica Section B* **1976**, *32*, (5), 1470-1476.
56. Alemi, A.; Soleimani, E.; Starikova, Z. A., The novel route for synthesis of tellurium tetrachloride, and redetermination of its structure at lower temperature by X-ray crystallography. *Acta Chimica Slovenica* **2000**, *47*, (1), 89-98.

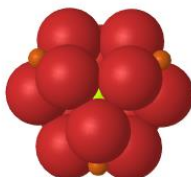
A_2BX_6 Structural Diversity



Cs_2SiF_6



Cs_2SnCl_6



Cs_2SnI_6